symmetry

MDPI

Article

Studying Alumina–Water Nanofluid Two-Phase Heat Transfer in a Novel E-Shaped Porous Cavity via Introducing New Thermal Conductivity Correlation

Taher Armaghani [1], Mojtaba Sepehrnia [2], Maysam Molana [3], Manasik M. Nour [4] and Amir Safari [5,*]

[1] Department of Mechanical Engineering, West Teran Branch, Islamic Azad University, Tehran 1468763785, Iran
[2] Department of Mechanical Engineering, Technical and Vocational University, Qom 3716146611, Iran
[3] Department of Mechanical Engineering, Wayne State University, Detroit, MI 48201, USA; molana@wayne.edu
[4] Department of Mathematics, College of Science and Humanities in Al-Karj, Prince Sattam bin Abdulaziz University, Al-Kharj 11942, Saudi Arabia
[5] Department of Science and Industrial Systems, University of Southeast Norway, 3616 Kongsberg, Norway
* Correspondence: amir.safari@usn.no

Abstract: Investigating natural convection heat transfer of nanofluids in various geometries has garnered significant attention due to its potential applications across several disciplines. This study presents a numerical simulation of the natural convection heat transfer and entropy generation process in an E-shaped porous cavity filled with nanofluids, implementing Buongiorno's simulation model. Analyzing the behavior of individual nanoparticles, or even the entire nanofluid system at the molecular level, can be extremely computationally intensive. Symmetry is a fundamental concept in science that can help reduce this computational burden considerably. In this study, nanofluids are frequently conceived of as a combination of water and Al_2O_3 nanoparticles at a concentration of up to 4% by volume. A unique correlation was proposed to model the effective thermal conductivity of nanofluids. The average Nusselt number, entropy production, and Rayleigh number have been illustrated to exhibit a decreasing trend when the volume concentration of nanoparticles inside the porous cavity rises; the 4% vol. water–alumina NFs yield 17.35% less average Nu number compared to the base water.

Keywords: nanofluids; natural convection; cavity; entropy generation; correlation; thermal conductivity

Citation: Armaghani, T.; Sepehrnia, M.; Molana, M.; Nour, M.M.; Safari, A. Studying Alumina–Water Nanofluid Two-Phase Heat Transfer in a Novel E-Shaped Porous Cavity via Introducing New Thermal Conductivity Correlation. *Symmetry* **2023**, *15*, 2057. https://doi.org/10.3390/sym15112057

Academic Editors: Victor A. Eremeyev and Constantin Fetecau

Received: 6 September 2023
Revised: 28 October 2023
Accepted: 9 November 2023
Published: 13 November 2023

1. Introduction

Thermal researchers and scientists have found nanofluids (NFs) interesting in the way of looking for new cooling methods to address the heat removal necessity in different industries and applications. Choi and Eastman [1] pioneered the utilization of NFs as a novel means to augment heat transfer (HT) efficiency in cooling processes, marking an unprecedented milestone in the history of thermal science. The notion of suspending small particles inside a conventional fluid to enhance its physical characteristics was first presented by Maxwell [2] during the nineteenth century. Maxwell's concept was to improve the physical characteristics of water by dispersing metal particles in it, but the rapid sedimentation of micro-particles hindered this vision. Over the past two decades, NFs have garnered significant attention from the scientific community, corporate entities, and funding organizations.

NFs are characterized as colloidal suspensions consisting of nanoparticles at the nanoscale dispersed within common HT fluids, which commonly include oil, ethylene glycol, and water.

Symmetry is a vital concept in the analysis of NFs. Symmetry in fluid dynamics refers to the existence of geometric or physical features that are preserved under certain transformations or operations. These symmetries can be broadly categorized into two types:

geometric symmetry and flow symmetry. Generally speaking, symmetry can significantly simplify the analysis and computation of fluid flow problems. This simplification has several important applications, including Reduction of Computational Time, Simplification of Boundary Conditions, and Enhanced Visualization and Insight. Furthermore, Symmetry remains vital in the analysis of NFs, as it can help simplify the computational modeling and understanding of fluid behavior at the nanoscale. Application of the symmetry concept can lead to significant computational efficiency gains, simplified boundary conditions, and a better understanding of the behavior of nanoparticles in NFs, ultimately contributing to the advancement of NF-based technologies and applications. Enhancing several thermophysical properties, such as density, viscosity, specific HT capacity, and thermal conductivity, is the main goal. Usually, metals or oxides and carbon nanotubes are utilized for developing nanoparticles. NFs have been utilized in various industries, especially heat exchangers [3–5], impingement jets [6–8], automotive [9], renewable energies [10–13], heating and tempering processes [14], nuclear reactors [15,16], electronic chip cooling [17,18], lubrication [19–22], and combustion [23], among others [24,25].

On the other side, cavities are heavily used in a variety of applications and machinery like HVACs [26,27], heat exchangers [28,29], renewable energies [30,31], etc. It appears that one of the early investigations pertaining to fluid flow within enclosed spaces was conducted by Patterson and Imberger [32]. Their study delved into the dynamics of unsteady natural convection within a rectangular cavity that possessed end walls with varying temperatures. They concluded that the Prandtl number heavily affects the transient flows. However, the steady-state flows are not impacted by the Prandtl number variation.

Chamkha et al. [33] studied the HT characteristics of single and hybrid nanoparticles suspended in phase-change materials around a heated horizontal cylinder within a square cavity numerically. Parameters such as the Fourier number, NF viscosity, thermal conductivity, and nanoparticle concentration were systematically varied. Their findings revealed that the rate of phase-change melting rises as the Fourier number rises up to a threshold value of 0.5. Beyond this threshold, a decrease in the melting rate was observed.

Selimefendigil and Oztop [34] carried out a numerical exploration of the effect of an inclined magnetic field on natural convection within a triangular enclosure characterized by internal heat generation. The Galerkin weighted residual finite element technique was utilized to solve the governing equations. Important parameters investigated in detail were the internal and exterior Rayleigh numbers, the elastic modulus of flexible wall tilt, the magnetic field strength (represented by the Hartmann number), and their combined effect on HT. Their analysis revealed that a rise in both the internal Rayleigh number and the Hartmann number corresponded to a reduction in the average HT rate.

The study carried out by Selimefendigil et al. [35] examined the interaction among fluid dynamics, structural elements, and a magnetic field within a lid-driven cavity containing NFs equipped with a flexible sidewall. Their analysis suggested that the mean Nusselt number significantly dropped as the Hartmann number boosted.

The present research relies on the finite volume approach to numerically analyze the HT by natural convection within an E-shaped porous enclosure filled with NFs. The NFs consist of water with an Al_2O_3 nanoparticle volume concentration of up to 4%. The analysis is carried out based on Buongiorno's model, assuming incompressible, laminar, steady-state, homogenous, Newtonian behavior of the NFs, and lastly, the thermal equilibrium between the nanoparticles and the molecules of the base fluid. The research paper uses experimental data from the literature to demonstrate a unique prediction correlation for effective thermal conductivity, given that HT in NFs is strongly connected to their thermophysical characteristics.

2. Materials and Methods

2.1. The Geometry of the Problem

The computational domain in this study is presented in Figure 1. This is an E-shaped porous enclosure saturated with NFs. All walls are stationary. The vertical walls located

on the right side of the enclosure exhibit low temperatures, whereas high temperatures characterize the left wall. The temperature of the hot and cold walls is adjusted to 327 and 325 degrees of kelvin, respectively. The insulation is on the remaining walls. The problem is meshed into 19,200 cells in total, or two cells per millimeter. The geometry is divided into eight distinct sections, including five sections for the column. The shown dimensions are in millimeter units.

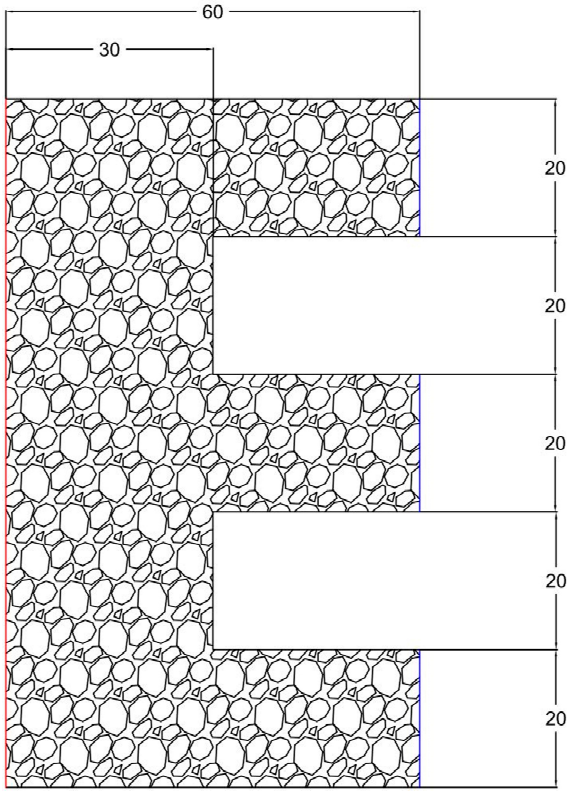

Figure 1. The problem geometry. The blue and red lines show the cold and hot walls.

2.2. Material

The NFs being examined in the present investigation are composed of alumina nanoparticles distributed in water, serving as the base fluid. The concentration of nanoparticles in the NFs varies from 0 to 4% by volume. The alumina nanoparticles are assumed to possess a mean diameter of approximately 33 nm, and it is noteworthy that no surfactants have been incorporated into the formulations. Table 1 contains reference values for a range of thermo-physical parameters about the water and alumina nanoparticles in ambient settings. Additionally, the porous media used in this study comprises two distinct compositions: sand and metallic powder. These materials exhibit distinct thermal conductivities with values of 3 W/m·K and 60 W/m·K, correspondingly. For analytical purposes, each of these two cases will be addressed separately. The porous media are characterized by a porosity of 0.4 and a permeability of 10^{-8} m^2.

Table 1. Thermo-physical properties of alumina nanoparticles and water at the ambient conditions [36,37].

Material	Thermal Expansion Coefficient (1/K)	Dynamic Viscosity (N.S/m^2)	Thermal Conductivity Coefficient (W/m.K)	Density (kg/m^3)	Specific Heat Capacity (J/kg.K)
Al_2O_3	0.00000846	-	40	3600	765
Water	0.000207	0.0001002	0.598	998.3	4179

2.3. Governing Equations

The assumptions in this problem are as follows:

- Incompressible fluid;
- Steady, laminar flow;
- Homogenous NFs;
- Two-dimensional flow;
- No chemical reactions;
- No viscous dissipation;
- No radiative HT;
- Homogenous porous media;
- Isentropic porous media;
- The primary mechanisms for nanoparticles' slip are Brownian diffusion and thermophoresis.
- In all prestigious books, one says that a fluid can be compressible or incompressible, while a motion or flow can be steady or unsteady (non-steady). In order to scrutinize the efficacy of nanoparticle slip in relation to the molecules of the base fluid, the equations that describe the conservation of mass and momentum are represented in the following manner:

  The mass conservation:

$$\vec{\nabla}.\left(\rho_{nf}\vec{V}\right) = 0 \tag{1}$$

  The momentum conservation:

$$\vec{\nabla}.\left(\rho_{nf}\vec{V}.\vec{V}\right) = -\vec{\nabla}(P) + \vec{\nabla}.(\mu_{nf}(\vec{\nabla}.\vec{V} + \vec{\nabla}.\vec{V^T})) + S_V \tag{2}$$

where the source term for porous media is denoted by S, which is specified as follows:

$$S_V = -\left(\mu_{nf}d\vec{V} + \frac{\rho_{nf}|V|f\vec{V}}{2}\right) \tag{3}$$

The Darcy coefficient and the Forchheimer coefficient are indicated by the variables d and f in this context, correspondingly. The following is the formal definition of these coefficients [38]:

$$d = \frac{\varepsilon}{K} \tag{4}$$

$$f = \frac{3.5}{\sqrt{150}\sqrt{K}\varepsilon^{0.5}} \tag{5}$$

The principle of energy conservation for NFs in a porous medium is described as [38]:

$$\rho_{nf}C_{Pnf} * \vec{V}.\vec{\nabla}T = \vec{\nabla}.\left(k_{eff}\vec{\nabla}T\right) + \varepsilon\rho_{np}C_{pnp}\left[D_B\vec{\nabla}\phi\vec{\nabla}T + D_T\frac{\vec{\nabla}T.\vec{\nabla}T}{T}\right] \tag{6}$$

The volume concentration of nanoparticles in NFs must adhere to the following equation [39], in which T_o, k_{eff}, ε, v, and B represent the mean temperature of the NFs, the effective thermal conductivity of the porous medium, porosity, the vectors of Darcy velocity, and thermal expansion coefficient, correspondingly. Furthermore, ρ, C_{pnp}, C_p, μ, ϕ, D_T, and D_B denote the density of NF, the specific heat of nanoparticles at constant pressure, the specific heat of NFs at constant pressure, the dynamic viscosity of NFs, the nanoparticle volume concentration, the thermophoresis coefficient, and the Brownian diffusion coefficient, respectively.

$$\frac{1}{\varepsilon}\vec{V}\cdot\vec{\nabla}\phi = \vec{\nabla}\cdot\left[D_B\vec{\nabla}\phi + \frac{D_T}{T}\vec{\nabla}T\right] \tag{7}$$

Equations (8) and (9), as defined in reference [40], provide a mathematical description of the thermophoresis coefficient and Brownian diffusion coefficient. The Boltzmann constant, the bulk temperature of the NFs, the mean diameter of the nanoparticles, the thermal conductivity of the base fluid, and the thermal conductivity of the nanoparticles are expressed by the symbols K_b, T, d_{np}, k_{bf}, and k_{np} in these equations, correspondingly.

$$D_B = \frac{K_b T}{3\pi\mu_{nf} d_{np}} \tag{8}$$

$$D_T = \left(\frac{0.26k_{bf}}{2k_{bf} + k_{np}}\right) \rightleftarrows \left(\frac{\mu_{nf}}{\rho_{nf}}\right)\varphi \tag{9}$$

The overall entropy generation can be determined by applying Equation (10) [41].

$$S_{gen} = \left(\frac{k_{eff}}{T_0^2}\right) \times \left(\left(\frac{\partial T}{\partial x}\right)^2 + \left(\frac{\partial T}{\partial y}\right)^2\right) + \frac{\mu_{nf}}{KT_o} \times (u^2 + v^2) + \frac{\mu_{nf}}{T_o} \times \left(2\left(\left(\frac{\partial u}{\partial x}\right)^2 + \left(\frac{\partial u}{\partial y}\right)^2\right)\right) + \left(\frac{\partial u}{\partial x} + \frac{\partial v}{\partial y}\right)^2 \tag{10}$$

The mean Nusselt number can be calculated by integrating the ratio of the thermal conductivity of NFs to that of the base fluid, as follows [41]:

$$Nu = \int -\left(\frac{k_{eff}}{k_{bf}}\right) \times \left(\frac{\partial\theta}{\partial n}\right) dn \tag{11}$$

In Equation (11), n is the direction that is orthogonal to the surface. The definition of dimensionless temperature is:

$$\theta = \frac{T - T_{cold}}{T_{hot} - T_{cold}} \tag{12}$$

The proportional equation could be employed to calculate the porous media's effective thermal conductivity.

$$k_{eff} = \varepsilon k_{nf} + (1 - \varepsilon)k_{solid} \tag{13}$$

The thermal conductivity of porous materials and the thermal conductivity of NFs are depicted by the variables k_{solid} and k_{nf} in Equation (13). The method for calculating NF density is as follows:

$$\rho_{nf} = \phi\rho_{np} + (1 - \phi)\rho_{bp} \tag{14}$$

where ρ_{bf} and ρ_{np} denote, accordingly, the base fluid's density and the density of the nanoparticles. To determine the effective dynamic viscosity of NFs, an empirical correlation [37] was utilized:

$$\frac{\mu_{nf}}{\mu_{bf}} = 1 + 4.93\phi + 222.4\phi^2 \tag{15}$$

The determination of the thermal expansion coefficient of NFs could be achieved by employing Equation (16).

$$\rho_{nf}\beta_{nf} = (1 - \phi)\rho_{bf} + \phi\rho_{np}\beta_{np} \tag{16}$$

2.4. A Novel Correlation for Thermal Conductivity

An innovative prediction correlation was formulated. Relying on empirical data reported in the literature, it was developed to determine the thermal effectivity of NFs. To this end, 40,182 data points about the thermal conductivity of alumina-based NFs were obtained from experimental research for developing a novel correlation model. Afterward,

the technique of Gauss–Newton multiple regression was employed. After performing 46 iterations, the equation suggested is expressed as follows (Equation (17)):

$$k_{nf} = k_{bf} \times (1 + (1.48185 \times \phi)^2 \times \frac{0.0363}{d_{np}}) \quad (17)$$

where k_{nf}, k_{bf}, φ, and d_{np} denote, accordingly, the effective thermal conductivity of the NFs (W/m.K), the base fluid's thermal conductivity (W/m.K), the volume concentration of the nanoparticles (%), and the mean diameter of the nanoparticles (nm). Additional statistical information on the proposed correlation is provided in Table 2. Compared to the empirical information, the mean absolute error of the intended correlation is 4.42%. Patel et al. [42], to validate the claimed correlation, carried a comparison analysis out utilizing data from an empirical investigation. The difference between the thermal conductivity predicted by the suggested correlation and the empirical results as a function of temperature is seen in Figure 2. The graphical representation shows that the experimental and predicted data exhibit a growing trend in effective thermal conductivity as the mean operating temperature increases.

Table 2. The statistical parameters.

Parameter		Value
1	Tolerance	0.00001
2	Iterations	17
3	Final SSE	213.429
4	DFE	35338
5	MSE	0.00603
6	S	0.07771

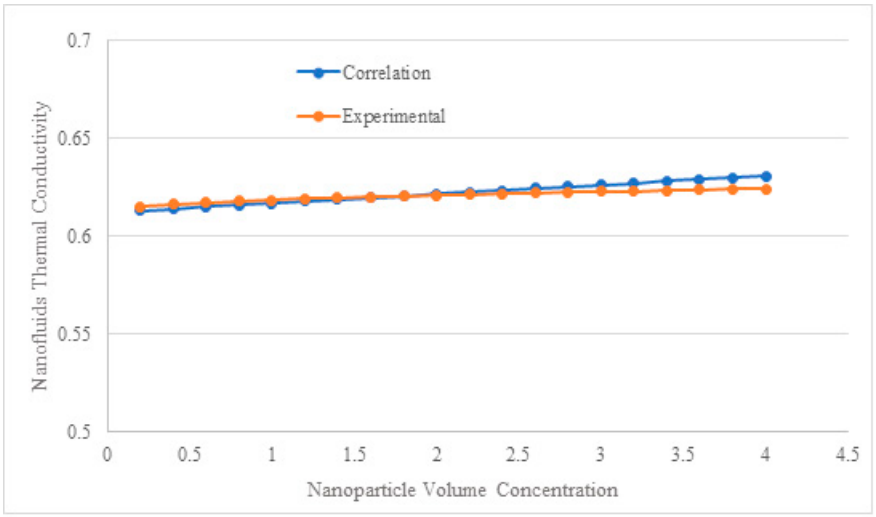

Figure 2. The experimental versus forecasted effective thermal conductivity by the presented correlation [42].

2.5. Numerical Method and Validation

We used the finite volume method for discretizing the governing equations in the OpenFOAM software package v1906, with some additional programmed code in C++ for considering thermophoresis, Brownian diffusion, and entropy generation. The solution mode is steady, employing a straightforward algorithm for solving the velocity and pressure coupling equations. To incorporate the pertinent relationships within the OpenFOAM software v1906, properties dependent on temperature, including density, viscosity, and conductivity coefficient, are initially specified in the createFields file. Subsequently, these

relationships undergo updates at the conclusion of the files associated with energy equations and volume fractions. To account for porosity effects, the fvOptions file is taken into consideration, and the fvOptions statement is integrated into the momentum equation. Darcy–Forchheimer coefficients are adjusted based on the sand's porosity and permeability in the aforementioned file. A convergence threshold of 10–6 is set for all parameters. Lastly, the groovy bc tool is utilized to implement the boundary condition in the OpenFOAM software v1906, addressing the absence of flux-related boundary conditions.

The validation process of the numerical methodology employed in this study was carried out in two phases, utilizing established reference data. Initially, the outcomes obtained for airflow within the cavity were juxtaposed with the findings presented by Davis [43]. The graphical representation in Figure 3 portrays the relationship between the Nusselt number and the Rayleigh number. The analysis of these results indicates that the maximum deviation from the reference data is 1.066%. Consequently, the numerical solution employed in this study can be considered highly accurate in the initial phase of validation.

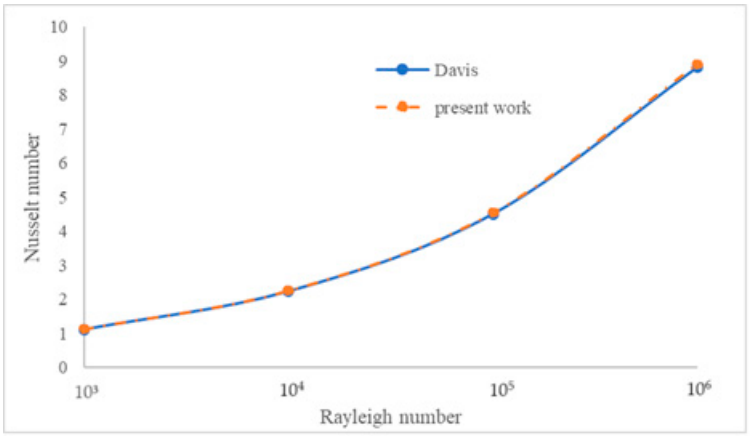

Figure 3. The comparison of the obtained results with reference [43].

The outcomes of the natural convection of NFs in a porous enclosure were compared with those obtained by Nithiarasu et al. [38] in the second step. The findings of the suggested numerical solution are displayed in Table 3, along with a comparison with the reference. As it can be concluded, the largest deviation from the reference value in the current study is 1.069%, producing extremely accurate findings. As a result, the inaccuracy diminishes as porosity and Rayleigh number rise.

Table 3. The comparison between the obtained results with the reference.

Rayleigh Number		Darcy Number	Porosity	Reference Nusselt Number [38]	Nusselt Number	Error
1	10^3	0.01	0.4	1.008	1.0208	1.069%
2	10^6	0.0001	0.6	2.725	2.7410	0.589%
3	10^4	0.01	0.9	1.640	1.6550	0.920%

2.6. Grid Independency Study

Seven alternative meshes were used in an extensive mesh testing approach to determine the right grid size for solving the present problem while taking into account constant variables like the Rayleigh number and nanoparticle volume concentration. Table 4 presents the results acquired using various mesh sizes. A comparison analysis of the computed average Nusselt numbers reveals that the average Nusselt number for a mesh configuration with 67,600 elements (260 × 260) differs by 0.32% from the conclusions drawn from the other element counts. As a result, it has been determined that, in the context of this research,

the mesh design with 6218 nodes and 67,600 elements satisfies the requirements for an accurate solution with appropriate grid independence.

Table 4. Test of the grid independence in the current investigation.

Nanoparticle Volume Concentration (%)		Rayleigh Number	Reference Nusselt Number [38]	Mesh Size	Clock Time (Sec)	Obtained Nusselt Number	Variation (%)
1	3	5.6×10^7	29.0769	140 × 140	334	29.2141	0.47
2	3	5.6×10^7	29.0769	160 × 160	651	28.8535	1.23
3	3	5.6×10^7	29.0769	180 × 180	940	28.5944	0.89
4	3	5.6×10^7	29.0769	200 × 200	1457	28.4005	0.67
5	3	5.6×10^7	29.0769	220 × 220	2209	28.2551	0.51
6	3	5.6×10^7	29.0769	240 × 240	3781	28.1401	0.40
7	3	5.6×10^7	29.0769	260 × 260	4247	28.0485	0.32

3. Results and Discussion

In this section, the acquired findings will be displayed and discussed. The mean nanoparticle diameter is assumed to be 33 nm, and the problem is solved five times for nanoparticle volume concentrations of 0%, 1%, 2%, 3%, and 4%, and the streamlines, isotherms, and entropy generation contours are obtained. Figure 4 shows the temperature distribution of the base fluid in natural convection. The isotherms also are shown, and all of them are perpendicular to the insulated walls. On the cavity's right side, the isotherms are denser. This demonstrates a developing temperature differential from the left to the right. Natural convection HT in NFs occurs at very slow velocities. In this context, the fluid flow and temperature distribution would show a layer profile, as it is shown in Figure 4.

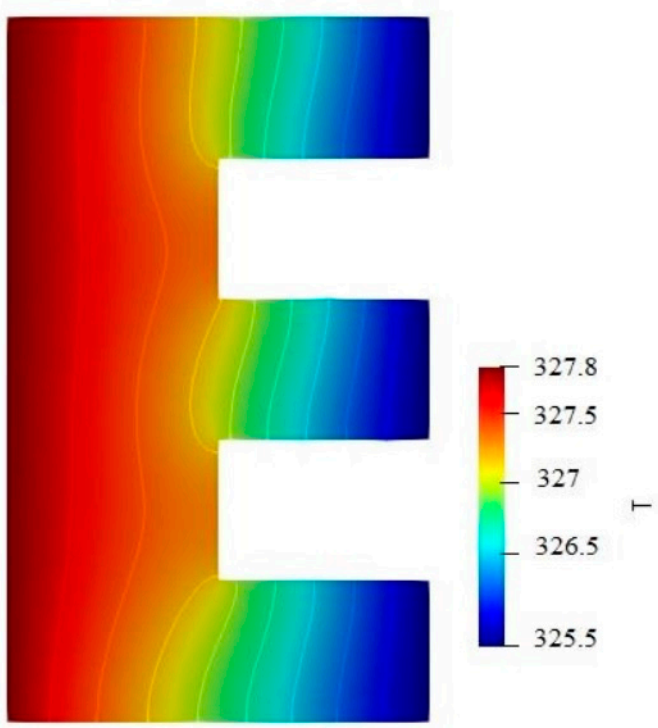

Figure 4. The temperature distribution of the 0% vol. NFs (base fluid).

Figure 5 also represents the streamlines of the base fluid under natural convection HT. As it is shown, there are three distinct cells in the column. The number of streamlines is

greater around the cells. This means that the fluid velocity is a considerable amount in these regions. The streamlines are also rare at the horizontal ends. The vorticities lead to higher velocities at the sharp corners of the E-shaped cavity.

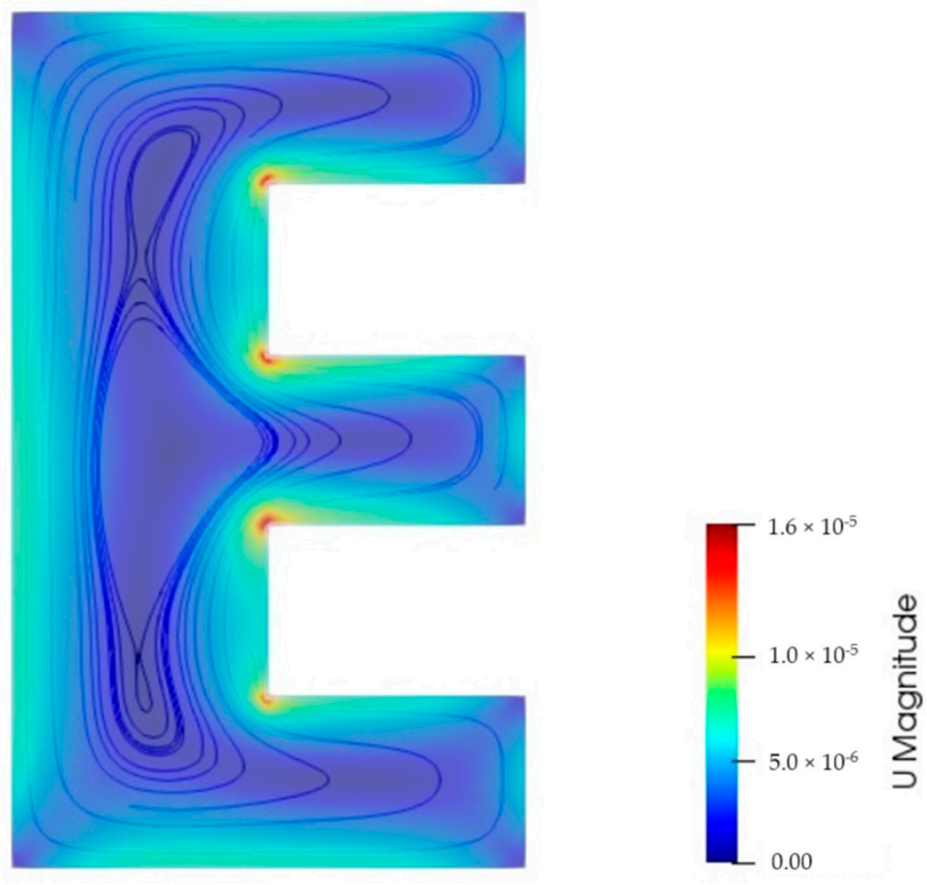

Figure 5. The streamlines of the 0% vol. NFs (base fluid).

The contours of entropy generation are shown in Figure 6 for the base fluid under natural convection. The internal corners of the geometry are where most entropy generation takes place. The number of constant entropy lines in these regions is greater than in the other regions. The entropy generation is also negligible in most areas of the column and is dominant in the horizontal ends of the geometry. As it was explained earlier, the higher velocities near the walls lead to an increase in fluid friction irreversibility. Furthermore, the temperature gradient is larger near the sharp corners. Therefore, irreversibility due to HT increases. In this context, total entropy grows in these regions, consequently.

Figure 7 shows the streamlines of the water–alumina NFs in natural convection for different nanoparticle volume concentrations. Increasing the nanoparticle volume concentration leads to separating the lower cell from the central cell. This is happening because of the increasing buoyancy force due to the more natural convection HT in a greater amount of the nanoparticle volume concentrations. The streamlines are also rotating clockwise within the cavity.

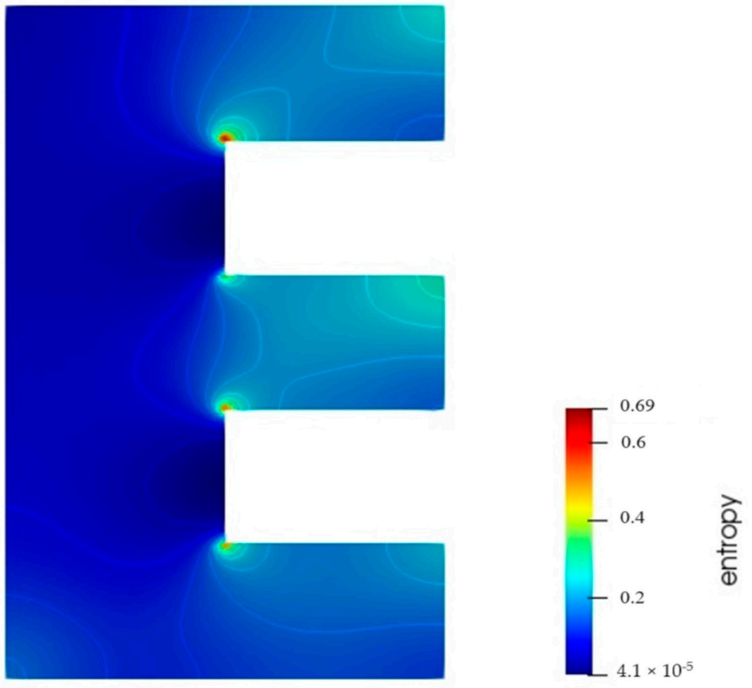

Figure 6. Entropy generation contour of the base fluid.

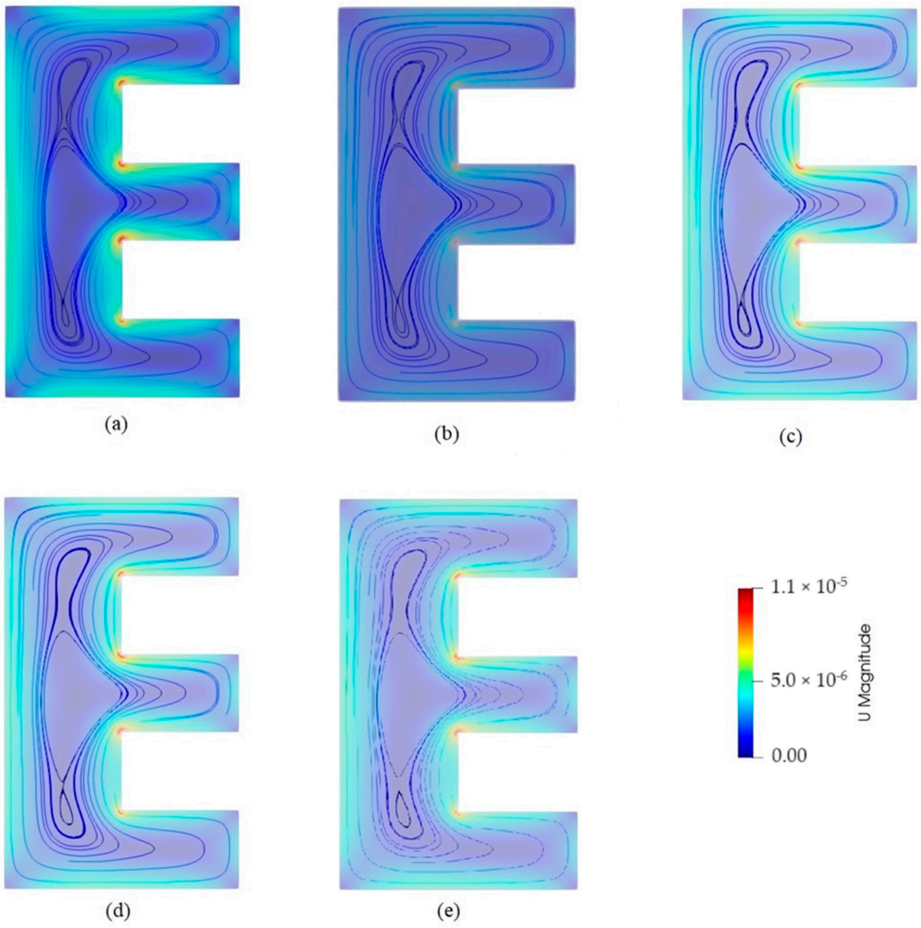

Figure 7. Streamlines of the water–alumina NFs in natural convection for different nanoparticle volume concentrations (**a**) 0%, (**b**) 1%, (**c**) 2%, (**d**) 3%, and (**e**) 4%.

The water–alumina NFs' entropy generation contours for varying nanoparticle volume concentrations are displayed in Figure 8. As it is shown, entropy generation increases with any rise in the volume concentration of the nanoparticle due to the reduction of irreversibility of the process and natural convection. More friction, more irreversibility, and therefore, more entropy generation is observed in the internal corners of the cavity. As Figure 7 suggests, the velocity gradient reduces as the nanoparticle volume concentration rises. Therefore, lower total entropy levels are expected near the walls.

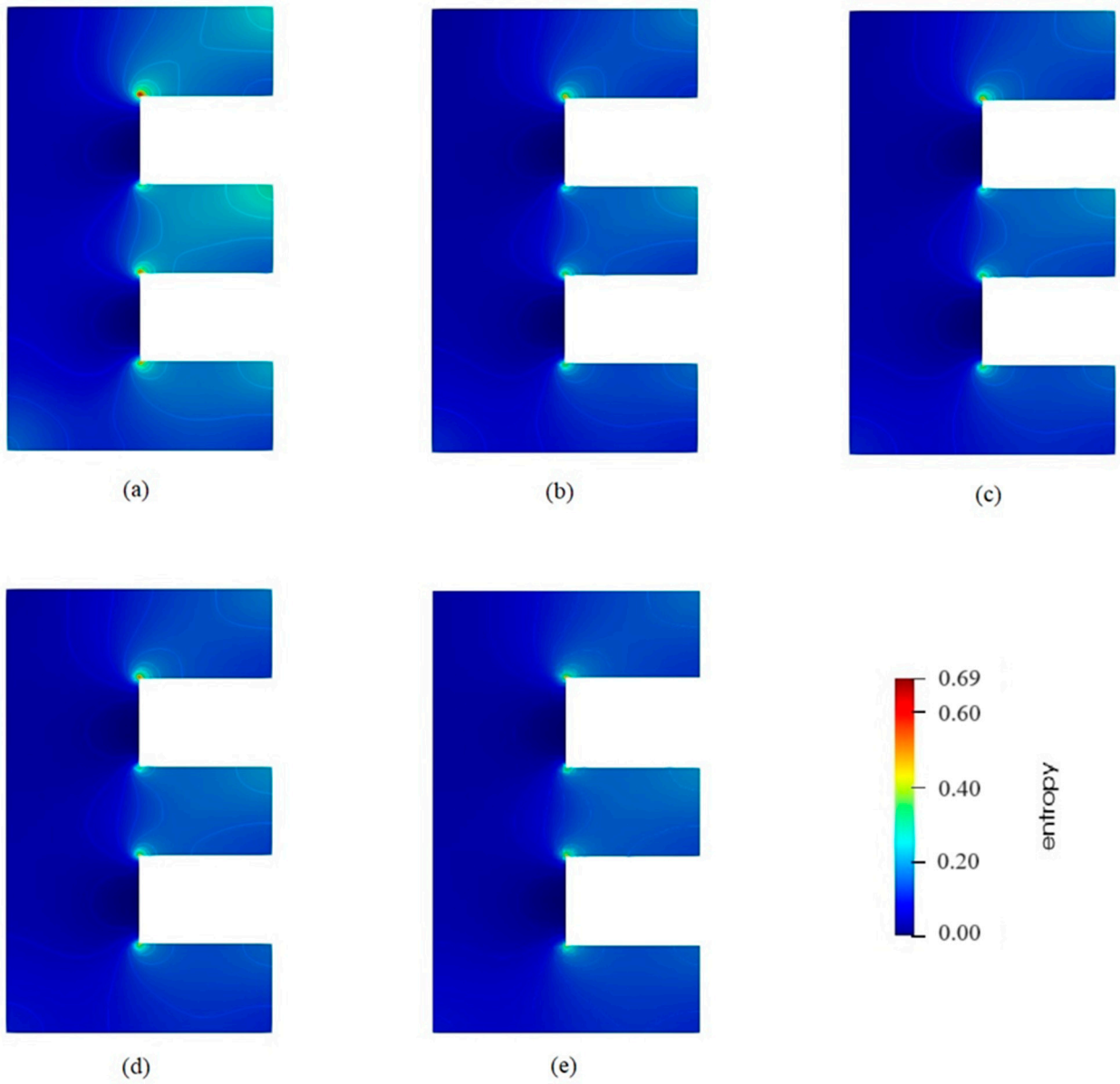

Figure 8. The entropy generation contours of the water–alumina NFs for different nanoparticle volume concentrations (**a**) 0%, (**b**) 1%, (**c**) 2%, (**d**) 3%, and (**e**) 4%.

Figure 9 shows the entropy generation of water–alumina/NFs with a mean diameter of 33 nm versus the nanoparticle volume concentration. The overall entropy generation decreases with increasing nanoparticle volume concentrations. For example, 4% vol. NFs give 1.4% less entropy generated than the base fluid.

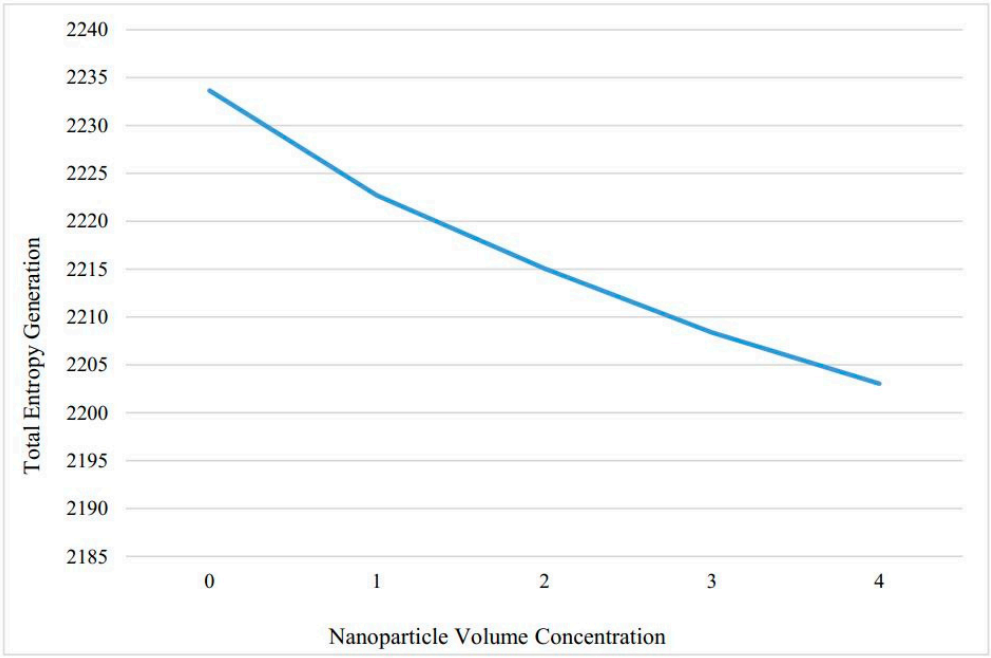

Figure 9. Entropy generation of water–alumina NFs with a mean diameter of 33 nm versus the nanoparticle volume concentration.

We also assessed how porosity influences the transfer of heat. Beforehand, we anticipated that the porosity of a low-conductivity material like glass would leave a considerable effect on the HT of NFs in natural convection. We solved the problem again with a porosity of 0 and 0.4. Therefore, we have two different media: a non-porous and a porous media with a high permeability. Figure 10 demonstrates the findings obtained for various nanoparticle volume concentrations. The findings indicated that the HT in the non-porous cavity boosts with any rise in the volume concentration of the nanoparticle. In contrast, in the non-porous cavity, 4% vol. NFs result in a 17.35% higher average Nusselt number than the base fluid.

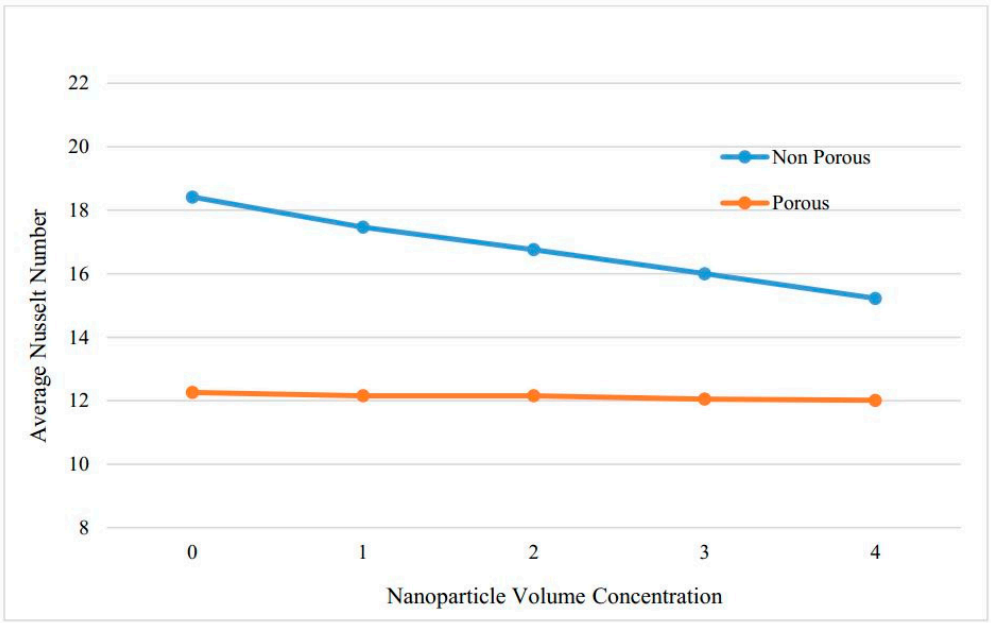

Figure 10. Average Nusselt number versus nanoparticle volume concentration for two different cases.

Any rise in the volume concentration of nanoparticles in the porous cavity additionally results in a reduction in the rate of HT. However, the decrement is considerably slower

in comparison to the non-porous cavity. The average Nusselt number for 4% vol. NFs in the porous cavity is 2.05% lower than in the non-porous cavity, according to the findings. Therefore, it could be concluded that porosity is the best option to control the natural convection HT.

4. Conclusions

This numerical study explores the natural convection HT characteristics of NFs within a porous E-shaped cavity. The NFs considered are assumed to be composed of water and Al_2O_3 nanoparticles, with volume concentrations ranging up to 4%. The problem is figured out by utilizing a finite volume method, implementing Buongiorno's approach, and making specific assumptions consisting of laminar flow, incompressibility, steady-state conditions, homogeneity, Newtonian behavior of NFs, and thermal equilibrium between nanoparticles and the molecules of the base fluid. To enhance accuracy, a correlation has been developed to predict the effective thermal conductivity of NFs utilizing a multi-variable regression technique. The principal findings of this investigation are summarized as follows:

1. An augmentation in the nanoparticle volume concentration could result in a reduction in entropy generation, average Nusselt number, and Rayleigh number of the porous cavity. In natural Convection, 4% vol. NFs are shown to give a 2.1% less average Nusselt value than the base fluid.
2. The HT performance of the non-porous cavity is highly dependent on the nanoparticle volume concentration. The 4% vol. water–alumina NFs yield is a 17.35% less average Nusselt number than the base water.
3. Porosity is an applicable method to control the natural convection HT.
4. The addition of nanoparticles to the base fluid results in a non-linear augmentation in the effective thermal conductivity of the NFs. The 4% vol. NFs give around 21% augmentation in effective thermal conductivity in comparison with the base fluid.

Author Contributions: Conceptualization, T.A. and A.S.; Methodology, T.A., M.S. and M.M.; Software, M.M.; Validation, M.M.N.; Formal analysis, T.A., M.S. and M.M.N.; Resources, T.A., M.S., M.M.N. and A.S.; Data curation, M.M.; Writing—original draft, T.A.; Writing—review & editing, M.S. and A.S.; Visualization, M.M.; Supervision, A.S.; Funding acquisition, M.M.N. All authors have read and agreed to the published version of the manuscript.

Funding: This research was funded by Prince Sattam bin Abdulaziz University, grant number (PSAU/2023/01/9055).

Data Availability Statement: Data are contained within the article.

Acknowledgments: Manasik M. Nour acknowledges with gratitude the support provided by Prince Sattam bin Abdulaziz University for financing this research endeavor.

Conflicts of Interest: The authors declare no conflict of interest.

Nomenclature

$\vec{V}$	Velocity vector
ρ_{nf}	Density of nanofluids
μ_{nf}	Dynamic viscosity of nanofluids
S	Source term for porosity
P	Pressure
d	Darcy coefficient
D_T	Coefficient of thermophoresis diffusion
D_B	Coefficient of Brownian diffusion
K_b	Boltzmann constant
d_{np}	Nanoparticle mean diameter

k_{bf}	Thermal conductivity of base fluid
k_{np}	Thermal conductivity of nanoparticle
S_{gen}	Entropy generation
ε	Porosity
u	Velocity component in X-direction
v	Velocity component in Y-direction
f	Forchheimer coefficient
K	Permeability
n	Normal vector
β_{nf}	Thermal expansion coefficient of nanofluids
β_{bf}	Thermal expansion coefficient of base fluid
β_{np}	Thermal expansion coefficient of nanoparticle
Nu	Nusselt number
T	Temperature
θ	Dimensionless temperature
T_0	Reference temperature (Mean temperature)
T_{cold}	Temperature at cold surface
T_{hot}	Temperature at hot surface
$C_{p,nf}$	Heat capacity of nanofluids at constant pressure
k_{eff}	Effective thermal conductivity of nanofluids
k_{solid}	Thermal conductivity of porous media
ρ_{np}	Density of nanoparticle
ρ_{bf}	Density of base fluid
φ	Nanoparticle volume concentration
μ_{bf}	Dynamic viscosity of base fluid
$C_{p,np}$	Heat capacity of nanoparticle at constant pressure
$C_{p,bf}$	Heat capacity of base fluid at constant pressure
HT	heat transfer
NF	Nanofluid

References

1. Sus, C.; Eastman, J.A. Enhancing thermal conductivity of fluids with nanoparticles. In Proceedings of the Emerging Technologies: Presented at The 1995 ASME International Mechanical Engineering Congress And Exposition, San Francisco, CA, USA, 12–17 November 1995; Argonne National Lab.: Lemont, IL, USA, 1995.
2. Maxwell, J.C. *Electricity and Magnetism*; Clarendon Press: Oxford, UK, 1873.
3. Asadi, A. A guideline towards easing the decision-making process in selecting an effective nanofluid as a heat transfer fluid. *Energy Convers. Manag.* **2018**, *175*, 1–10. [CrossRef]
4. Hoseinzadeh, S.; Sahebi, S.A.R.; Ghasemiasl, R.; Majidian, A.R. Experimental analysis to improving thermosyphon (TPCT) thermal efficiency using nanoparticles/based fluids (water). *Eur. Phys. J. Plus* **2017**, *132*, 197. [CrossRef]
5. Qashqaei, A.; Asl, R.G. Numerical Modeling And Simulation Of Copper Oxide Nanofluids Used In Compact Heat Exchangers. *Int. J. Mech. Eng.* **2015**, *4*, 1–8.
6. Wongcharee, K.; Chuwattanakul, V.; Eiamsa-Ard, S. Influence of CuO/water nanofluid concentration and swirling flow on jet impingement cooling. *Int. Commun. Heat Mass Transf.* **2017**, *88*, 277–283. [CrossRef]
7. Li, Q.; Xuan, Y.; Yu, F. Experimental investigation of submerged single jet impingement using Cu–water nanofluid. *Appl. Therm. Eng.* **2012**, *36*, 426–433. [CrossRef]
8. Selimefendigil, F.; Öztop, H.F. Effects of Nanoparticle Shape on Slot-Jet Impingement Cooling of a Corrugated Surface With Nanofluids. *J. Therm. Sci. Eng. Appl.* **2017**, *9*, 021016. [CrossRef]
9. Leong, K.; Saidur, R.; Kazi, S.; Mamun, A. Performance investigation of an automotive car radiator operated with nanofluid-based coolants (nanofluid as a coolant in a radiator). *Appl. Therm. Eng.* **2010**, *30*, 2685–2692. [CrossRef]
10. Sui, D.; Langåker, V.H.; Yu, Z. Investigation of Thermophysical Properties of Nanofluids for Application in Geothermal Energy. *Energy Procedia* **2017**, *105*, 5055–5060. [CrossRef]
11. Nasrin, R.; Alim, M.; Chamkha, A. Effects of physical parameters on natural convection in a solar collector filled with nanofluid. *Heat Transf.* **2012**, *42*, 73–88. [CrossRef]
12. Asadi, A.; Rahbar, N.; Rezaniakolaei, A.; Rosendahl, L.A. Introducing a novel method to estimate the total heat transfer coefficient inside irregular-shape cavities utilizing thermoelectric modules; Special application in solar engineering. In Proceedings of the 36th International Conference on Thermoelectrics-ICT2017, Pasadena, CA, USA, 30 July–3 August 2017.
13. Rahbar, N.; Esfahani, J.A.; Asadi, A. An experimental investigation on productivity and performance of a new improved design portable asymmetrical solar still utilizing thermoelectric modules. *Energy Convers. Manag.* **2016**, *118*, 55–62. [CrossRef]

14. Alsabery, A.; Chamkha, A.; Saleh, H.; Hashim, I.; Chanane, B. Effects of finite wall thickness and sinusoidal heating on convection in nanofluid-saturated local thermal non-equilibrium porous cavity. *Phys. A Stat. Mech. Its Appl.* **2017**, *470*, 20–38. [CrossRef]
15. Siddiqui, O.K.; Shams, A.; Al-Athel, K. A Comprehensive Review on the Use of Nanoparticles in Nuclear Power Plants. *Arab. J. Sci. Eng.* **2023**, 1–25. [CrossRef]
16. Zubair, M.; Elgack, O.; Said, Z. Implications of using nanoparticles on the performance and safety of nuclear systems. *Nucl. Eng. Des.* **2023**, *414*, 112618. [CrossRef]
17. Asadi, A.; Asadi, M.; Rezaniakolaei, A.; Rosendahl, L.A.; Afrand, M.; Wongwises, S. Heat transfer efficiency of Al_2O_3-MWCNT/thermal oil hybrid nanofluid as a cooling fluid in thermal and energy management applications: An experimental and theoretical investigation. *Int. J. Heat Mass Transf.* **2018**, *117*, 474–486. [CrossRef]
18. Chu, Y.-M.; Farooq, U.; Mishra, N.K.; Ahmad, Z.; Zulfiqar, F.; Yasmin, S.; Khan, S.A. CFD analysis of hybrid nanofluid-based microchannel heat sink for electronic chips cooling: Applications in nano-energy thermal devices. *Case Stud. Therm. Eng.* **2023**, *44*, 102818. [CrossRef]
19. Lee, P.-H.; Nam, J.S.; Li, C.; Lee, S.W. An experimental study on micro-grinding process with nanofluid minimum quantity lubrication (MQL). *Int. J. Precis. Eng. Manuf.* **2012**, *13*, 331–338. [CrossRef]
20. Ettefaghi, E.-O.; Ahmadi, H.; Rashidi, A.; Nouralishahi, A.; Mohtasebi, S.S. Preparation and thermal properties of oil-based nanofluid from multi-walled carbon nanotubes and engine oil as nano-lubricant. *Int. Commun. Heat Mass Transf.* **2013**, *46*, 142–147. [CrossRef]
21. Asadi, A.; Asadi, M.; Rezaniakolaei, A.; Rosendahl, L.A.; Wongwises, S. An experimental and theoretical investigation on heat transfer capability of Mg (OH) 2/MWCNT-engine oil hybrid nano-lubricant adopted as a coolant and lubricant fluid. *Appl. Therm. Eng.* **2018**, *129*, 577–586. [CrossRef]
22. Asadi, A.; Asadi, M.; Rezaei, M.; Siahmargoi, M.; Asadi, F. The effect of temperature and solid concentration on dynamic viscosity of MWCNT/MgO (20–80)–SAE50 hybrid nano-lubricant and proposing a new correlation: An experimental study. *Int. Commun. Heat Mass Transf.* **2016**, *78*, 48–53. [CrossRef]
23. Ao, W.; Fan, Z.; Gao, Y.; Wang, Y.; Liu, P.; Li, L.K. Ignition and combustion characteristics of boron-based nanofluid fuel. *Combust. Flame* **2023**, *254*, 112831. [CrossRef]
24. Choudhury, R.; Das, U.J.; Ceruti, A.; Piancastelli, L.; Frizziero, L.; Zanuccoli, G.; Daidzic, N.E.; Rocchi, I.; Casano, G.; Piva, S. Visco-elastic effects on the three dimensional hydrodynamic flow past a vertical porous plate. *Int. Inf. Eng. Technol. Assoc.* **2013**, *31*, 1–8.
25. Samanpour, H.; Ahmadi, N.; Jabbary, A. Effects of applying brand-new designs on the performance of PEM fuel cell and water flooding phenomena. *Iran. J. Chem. Chem. Eng.* **2022**, *41*, 618–635.
26. Selimefendigil, F.; Öztop, H.F. Mixed convection of nanofluids in a three dimensional cavity with two adiabatic inner rotating cylinders. *Int. J. Heat Mass Transf.* **2018**, *117*, 331–343. [CrossRef]
27. Adeleye, S.A.; Oni, T.O.; Oluwaleye, I.O. Numerical Investigation of Temperature and Air Velocity Distribution in a Rectangular Cavity with Insulated Side Walls. *Int. J. Heat Technol.* **2023**, *41*, 891–900. [CrossRef]
28. Ferhi, M.; Abidi, S.; Djebali, R.; Mebarek-Oudina, F. Assessment of micro-scale heat exchangers efficiency using lattice Boltzmann method and design of experiments. *Energy Built Environ.* 2023.
29. Hou, T.; Xu, D. Pressure drop and heat transfer performance of microchannel heat exchangers with elliptical concave cavities. *Appl. Therm. Eng.* **2023**, *218*, 119351. [CrossRef]
30. Marandi, O.F.; Ameri, M.; Adelshahian, B. The experimental investigation of a hybrid photovoltaic-thermoelectric power generator solar cavity-receiver. *Sol. Energy* **2018**, *161*, 38–46. [CrossRef]
31. Nayak, J.; Agrawal, M.; Mishra, S.; Sahoo, S.S.; Swain, R.K.; Mishra, A. Combined heat loss analysis of trapezoidal shaped solar cooker cavity using computational approach. *Case Stud. Therm. Eng.* **2018**, *12*, 94–103. [CrossRef]
32. Patterson, J.; Imberger, J. Unsteady natural convection in a rectangular cavity. *J. Fluid Mech.* **1980**, *100*, 65–86. [CrossRef]
33. Chamkha, A.; Doostanidezfuli, A.; Izadpanahi, E.; Ghalambaz, M. Phase-change heat transfer of single/hybrid nanoparticles-enhanced phase-change materials over a heated horizontal cylinder confined in a square cavity. *Adv. Powder Technol.* **2017**, *28*, 385–397. [CrossRef]
34. Selimefendigil, F.; Öztop, H.F. Natural convection in a flexible sided triangular cavity with internal heat generation under the effect of inclined magnetic field. *J. Magn. Magn. Mater.* **2016**, *417*, 327–337. [CrossRef]
35. Selimefendigil, F.; Öztop, H.F.; Chamkha, A.J. Fluid–structure-magnetic field interaction in a nanofluid filled lid-driven cavity with flexible side wall. *Eur. J. Mech.—B/Fluids* **2017**, *61*, 77–85. [CrossRef]
36. Saghir, M.Z.; Ahadi, A.; Mohamad, A.; Srinivasan, S. Water aluminum oxide nanofluid benchmark model. *Int. J. Therm. Sci.* **2016**, *109*, 148–158. [CrossRef]
37. Ho, C.; Liu, W.; Chang, Y.; Lin, C. Natural convection heat transfer of alumina-water nanofluid in vertical square enclosures: An experimental study. *Int. J. Therm. Sci.* **2010**, *49*, 1345–1353. [CrossRef]
38. Nithiarasu, P.; Ravindran, K. A new semi-implicit time stepping procedure for buoyancy driven flow in a fluid saturated porous medium. *Comput. Methods Appl. Mech. Eng.* **1998**, *165*, 147–154. [CrossRef]
39. Nithiarasu, P.; Seetharamu, K.; Sundararajan, T. Natural convective heat transfer in a fluid saturated variable porosity medium. *Int. J. Heat Mass Transf.* **1997**, *40*, 3955–3967. [CrossRef]

40. Buongiorno, J. A non-homogeneous equilibrium model for convective transport in flowing nanofluids. In Proceedings of the ASME 2005 Summer Heat Transfer Conference collocated with the ASME 2005 Pacific Rim Technical Conference and Exhibition on Integration and Packaging of MEMS, NEMS, and Electronic Systems, San Francisco, CA, USA, 17–22 July 2005; pp. 1–9. [CrossRef]
41. Armaghani, T.; Ismael, M.A.; Chamkha, A.J. Analysis of entropy generation and natural convection in an inclined partially porous layered cavity filled with a nanofluid. *Can. J. Phys.* **2016**, *95*, 238–252. [CrossRef]
42. Patel, H.E.; Sundararajan, T.; Das, S.K. An experimental investigation into the thermal conductivity enhancement in oxide and metallic nanofluids. *J. Nanoparticle Res.* **2010**, *12*, 1015–1031. [CrossRef]
43. De Vahl Davis, G. Natural convection of air in a square cavity: A bench mark numerical solution. *Int. J. Numer. Methods Fluids* **1983**, *3*, 249–264. [CrossRef]